Methods S1. Detailed methods for optimal transport and mechanical model of tension propagation. Related to Figure 5, Figure 6, Figure S5.

1 Inference of surface flows with optimal transport

In this part, we derive the procedure for inferring membrane and actin flows from time-varying kymographs of their fluorescence intensity at the cell surface.

1.1 Kymographs generation

Raw kymographs

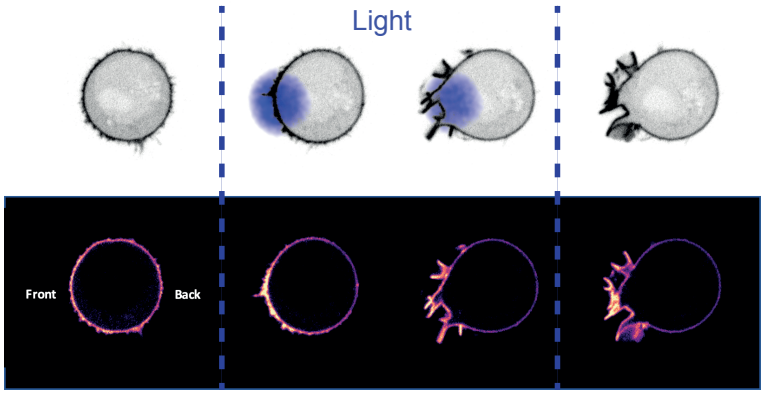

Example of membrane intensity fluorescent microscopy images during an optogenetic experiment.

Our optogenetics procedure aims at inducing endogenous cell surface perturbations by illuminating light-excitable proteins in a given time window. These deformations were observed by staining the membrane or the actin cortex with a fluorescent marker (CAAX-HaloTag & Actin-HaloTag) as shown above (see Methods). Normalized kymographs such as that shown in Fig. 4B or S4G, are generated from 2D fluorescent timelapse images of membrane or actin by computing the distribution of membrane intensity across the contour of the cells. Images are first translated and rotated to have the center of the optogenetic activation zone always at the same point and the cell deformation in the same direction. Movies are segmented using cellpose, a deep-learning tool [1], then distributions of intensity are built by using an histogram where the $n = 800$ bins constituted regularly spaced angular sectors of the cells, centered around the centroid of the pixels of the segmented membrane.

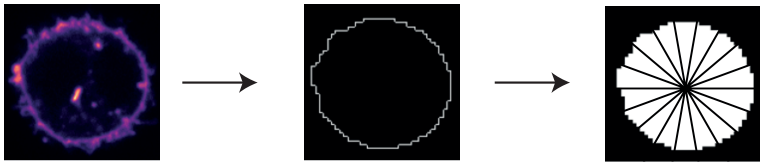

Segmentation of microscopy images and quantification of intensity by binning of the cell contour.

Total membrane and actin intensities are conserved in time

To observe membrane and actin flows, we imaged jointly membrane and actin intensities in experiments (Fig. 4A,S4F). With the procedure introduced previously, we derived kymographs of membrane and actin evolution across time (Fig. 4B, S4G). When plotting the average intensity, we observed that the total

intensity of the membrane or actin signals, integrated over the cell contour, is conserved across the time of one experiment (Fig. S4H).

1.2 Flow model

On the kymograph previously established, one may observe that at first, the distribution of membrane is uniform. After the illumination, the distribution becomes peaked at the front of the cell, becoming weaker at the back of the cell, before recovering to a uniform distribution after the illumination is stopped.
From this visual analysis, several questions arise:

- What kind of information can we extract from these observations?
- What kind of hypothesis are needed to infer a flow field?

We will introduce a simple model to describe flow. Given an initial distribution and a time and spatial-varying velocity field, we can generate kymographs, i.e a table describing the history of the evolution of the flow. Inverting this model will allow us to infer the flows.

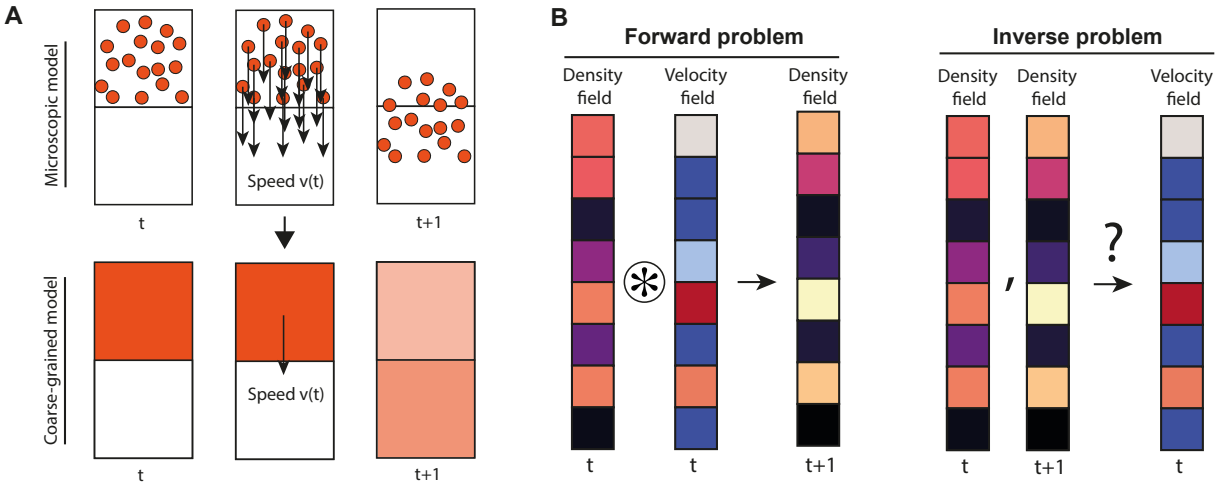

Introduction of the mathematical model used to infer flows from kymographs. a) *Spatial averaging of independent fluorophore intensities leads to a flow model where the concentration at each discrete spatial position evolves depending on the velocity attached to it* **b)** *Forward and inverse problems*

1.2.1 Microscopic model

A discrete kymograph is defined by dividing the space into a finite number n of discrete boxes of spatial coordinates $x_k = k\Delta x$ ($k \in \mathbb{Z}/n\mathbb{Z}$) and the time in discrete time steps separated by a sampling time Δt. Inside each of these boxes, we hypothesize that a large number of fluorescent particles are present at random positions x. Biologically speaking, the particles are proteins tagged with a fluorophore such as GFP, and they are transported with a time-variable velocity $v(x,t)$. Depending on their initial position, they can either remain into their initial box, or land into a neighboring one between a time t and a time $t + \Delta t$. Here, we assume the temporal sampling frequency high enough (i.e. the sampling time Δt small enough) such that, during a time Δt, a fluorophore will not travel a distance larger than the spatial sampling size Δx. For an ensemble of fluorescent particles, we can define the normalized velocity $\bar{v}(x,t) = |v(x,t)|\frac{\Delta t}{\Delta x}$. If $\Delta t \lesssim \Delta x / v_{\max}$, where $v_{\max}$ is the maximum velocity of a particle in the box, the normalized velocity measures a local probability for a particle to leave the box. This condition implies that our sampling time must be adapted to the velocity scale and small enough with respect to the sampling size.

If one can observe each particle and assign them a discrete position given the box in which they fall into, we will have:

- If $v(x,t) > 0$:

$$x(t + \Delta t) = x(t) + \Delta x \text{ with a probability } \bar{v}(x,t) \text{ and } x(t + \delta t) = x(t) \text{ with a probability } 1 - \bar{v}(x,t)$$

- If $v(x,t) < 0$:

  $x(t+\Delta t) = x(t) - \Delta x$ with a probability $\bar{v}(x,t)$ and $x(t+\delta t) = x(t)$ with a probability $1 - \bar{v}(x,t)$

1.2.2 Coarse-grained model

With classical fluorescence microscopy, following the displacement of each individual fluorophore is usually out of reach. We observe instead an average intensity,which represents the sum of individual fluorophores. Assuming a relatively uniform distribution of particles inside each box at each time step, the previous microscopic model allows us to describe in a coarse-grained manner the effect of a flow velocity $v(x_k,t)$ on an initial concentration $\mu^t(x_k)$, where the space is discretized as $x_k = k\Delta x$ ($k \in \mathbb{Z}/n\mathbb{Z}$). To do so, we define a normalized velocity field, average of the true velocity of all fluorophores in each box located at x_k as $V^t(x_k) = \int_{x_k-\Delta x/2}^{x_k+\Delta x/2} |v(x,t)| \frac{\Delta t}{\Delta x^2} \mathrm{d}x$. Following our reasoning above, this normalized velocity field also describes the fraction of particles that will jump to the next box x_{k+1} (or to the previous one if $v(x,t) < 0$) in a time Δt, while a fraction $1 - \bar{V}^t(x_k)$ will remain in its initial box centered at x_k.

If we consider the concentration field of particles $\mu^t(x_k)_{x_k \in \mathbb{Z}/n\mathbb{Z}}$, and a normalized velocity field $V^t(x)_{x \in \mathbb{Z}/n\mathbb{Z}}$, the evolution of the concentration may be cast into a master equation, for all k:

$$\begin{aligned} \mu^{t+\Delta t}(x_k) = \mathcal{F}[\mu^t, V^t](x_k) = \mu^t(x_{k-1}) V^t(x_{k-1}) \mathbb{1}_{V^t(x_{k-1})>0} \\ + \mu^t(x_{k+1}) V^t(x_{k+1}) \mathbb{1}_{V^t(x_{k+1})<0} \\ + \mu^t(x_k)(1 - |V^t(x_k)|) \end{aligned} \tag{1}$$

where $\mathbb{1}_{V^t(x)>0}$ and $\mathbb{1}_{V^t(x)<0}$ are indicator functions that are 1 when $V^t(x) > 0$, respectively $V^t(x) < 0$ and 0 otherwise.

1.2.3 Flow inference

When we observe the distributions of membrane intensity at two consecutive time steps μ^t and $\mu^{t+\Delta t}$, we observe that there has been a collective displacement of the particles between the two positions. To determine which particle goes where on average, we want to invert the master equation (1): given the fields μ^t and $\mu^{t+\Delta t}$, find V^t such that $\forall k \in \mathbb{Z}/n\mathbb{Z}, \mu^{t+\Delta t}(x_k) = \mathcal{F}[\mu^t, V^t](x_k)$.

This is a complicated inverse problem, due to the fact that the above expression changes with the sign of $V^t(x)$. Moreover, it is ill-posed: the solution is not unique and there is generally an infinite number of velocity fields that can explain the temporal evolution of the intensity distributions. To regularise this inverse problem, we will implement prior knowledge based on physical principles.

A first important physical hypothesis is that there is a notion of dissipation associated here to the flow. This dissipation is modeled by a cost function that we aim at minimizing. This is physically a fair hypothesis for inferring the flows of the membrane, that we consider throughout our manuscript as limited by the relative friction with the cortex (see model description in Section 2 of this Supplementary Text). We therefore choose a cost function that depends on local the velocity v_P of the path P as $\mathcal{C} \propto v_P^2$, which is consistent with a classical frictional dissipation. The local concentration of fluorophores being good indicator of the membrane density and, as a consequence, of the number of friction points, the local dissipation cost is furthermore expected to be proportional to the local concentration and we define $\mathcal{C}^t(x) = \mu^t(x)|V^t(x)|^2$.

We now reformulate the flow inference problem between two time steps t and $t+\Delta t$ as a minimisation of a cost function under the constraint of the master equation (1):

$$\min_{V^t \text{ s.t } \mathcal{F}(\mu^t, V^t) = \mu^{t+\Delta t}} \sum_k \mu^t(x_k) |V^t(x_k)|^q \tag{2}$$

where $q = 2$ corresponds to the physically-informed cost function $\mathcal{C}^t(x) = \mu^t(x)|V^t(x)|^2$.

Remarking that the time Δt between two sampling points remains the same, we can alternatively express the dissipation cost as function of the length l_P of the path P, as far as it remains small: $\mathcal{C}^t(x) = \mu_t(t) \frac{l_P(x)^2}{\Delta t^2}$

We propose below a way to solve this constrained optimisation problem using optimal transport. In fact, this method allows us to solve this problem for any $q \in \mathbb{R}$ in equation (2).

1.3 Optimal transport

1.3.1 Introduction: continuous transportation theory

Constrained optimisation problems as formulated in equation (2) can be cast into the generic class of optimal transport problems, which is a mathematical field formalized by Gaspard Monge in 1781 [2]. The problem was revisited in 1942 by Leonid Kantorovich who gave it its contemporary formulation [3].

To introduce shortly the optimal transport formulation, we first define a distance function $d(\cdot,\cdot)$, that takes as arguments two spatial positions along the membrane and returns a scalar value that represents the distance between two points. We write $c(\cdot,\cdot)$ the cost function that takes as arguments spatial positions along the membrane and returns a scalar value that represents the cost to go from one place to another. In the following, we will use $c(\cdot,\cdot) = d^q(\cdot,\cdot)$. We call the transport m a map such that $m(\mu^t) = \mu^{t+1}$.

In continuous settings, we want to find the optimal transport m^* that minimizes:

$$\min_{m, m(\mu^t)=\mu^{t+1}} \int c(x, m(x)) d\mu^t(x), \tag{3}$$

where the integration is done on the probability measure $\mu^t(x)$.

The optimal cost $W_c(\mu^t, \mu^{t+1}) = \int c(x, m^*(x)) d\mu^t(x)$ is called the Wasserstein distance between two measures. Here we are more interested on the mapping on itself, that is called the optimal transport matrix. Indeed, as this matrix gives a notion of distance traveled at each point on the membrane, we will determine the speed of the membrane flows using these discrete displacements.

1.3.2 Discrete optimal transport

Here we study discrete distributions. Following the notations of [4], we define a cost matrix C, a transport matrix M and a distance matrix D, (Fig. S4Ib-d), discretized versions of their continuous surrogates $c(\cdot,\cdot)$, $m(\cdot)$ and $d(\cdot,\cdot)$. For each discrete boxes i and j, of positions x_i and x_j, we have : $D_{i,j} = d(x_i, x_j)$. The cost matrix is defined generally as $C_{i,j} = |D_{i,j}|^q = |d^q(x_i, x_j)|$, following the. We write $\mathbb{1}$ the column vector where each value is one. For two simple distributions a and b, the optimal transport M^* is defined by:

$$M^* = \underset{M \in \mathbb{R}^{m \times n}}{\operatorname{argmin}} \sum_{i,j} M_{i,j} C_{i,j} \quad s.t. \quad M\mathbb{1} = a; M^T\mathbb{1} = b; \forall (i,j), M_{i,j} > 0 \tag{4}$$

We compute the optimal transport M^* using the standard Earth Mover's Distance (EMD) with [4]. This exact computation does not scales well with the number of boxes n (It has a $O(n^3)$ complexity [5]) but the 1D case has a low enough number of points to obtain results in a reasonable amount of time.

The velocity field V is obtained by averaging the distance traveled for every element, and dividing by the timestep Δt (Fig S4I.d):

$$\forall i, V_i = \frac{1}{\Delta t} (D_i \star M_i / a)^T \times \mathbb{1} \tag{5}$$

Where $\star$ is an element-wise multiplication, / the element wise division and $\times$ is the standard matrix product. X_i denotes the ith column of the matrix $X_{i,j}$.

1.3.3 Optimal transport with periodic boundary conditions

In our use-case, the cells are circular, and thus our distributions have periodic boundary conditions. One can travel along the membrane using a clockwise and an anticlockwise path. To account for this periodicity into account, we adapted the cost and distances matrices as shown on the figure below. Moreover, we decided to compute algebraic distances (i.e positive or negative values), to determine the direction of the flow from its sign (Fig. 4D,S4K).

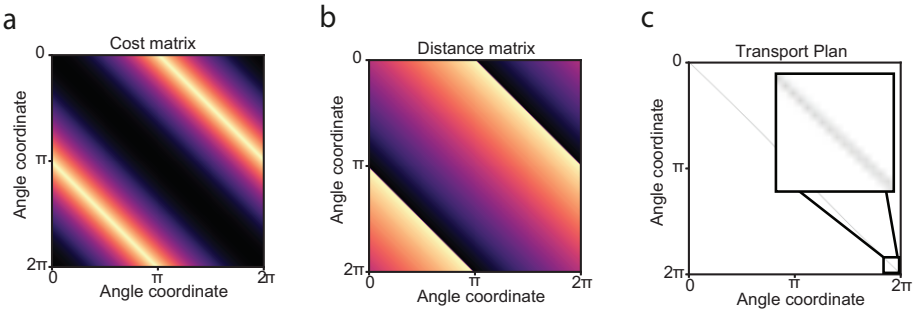

Modified cost and distance matrices to account for the periodic domain. a) *Modified cost matrix.* **b)** *Modified distance matrix.***b)** *Inferred transport plan.*

1.3.4 Numerical validation

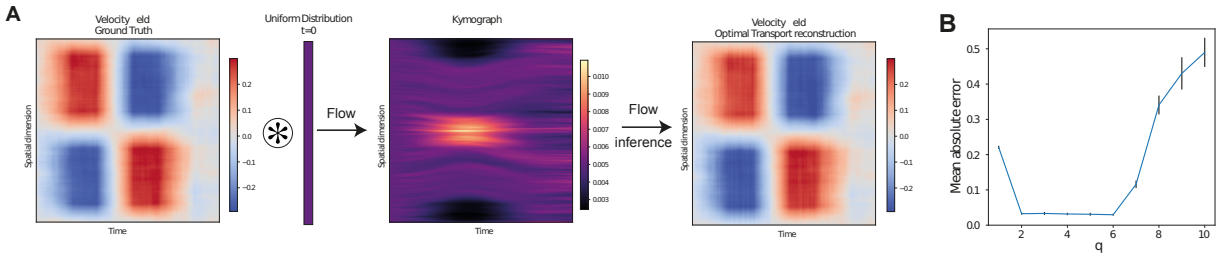

Numerical validation of the flow inference. a)*Pipeline of flow inference validation: kymographs are generated from a uniform initial distribution, and infered using optimal transport* **b)***On 20 different velocity fields, flows are infered with various values of q. The error is close to 0 with q ranging from 2 to 6*

To valid our procedure numerically, we generated velocity fields. Given an initial uniform distribution, we generate a kymograph from it using our master equation. The optimal transport problem allows us to infer the flow with little error in general. We tried it with different q as defined for the generic cost function in (2) and above. We see that for q ranging from 2 to 6, we roughly obtain the same error, whereas the error grows rapidly for $q \leq 1$ and $q \geq 7$. In the next, we will stick to $q = 2$ as this choice has a real physical meaning.

We show below 4 other numerical validation examples, where we followed the same procedure: Generation of a velocity field, computation of a kymograph from it, retrieval of the velocity field from the kymograph.

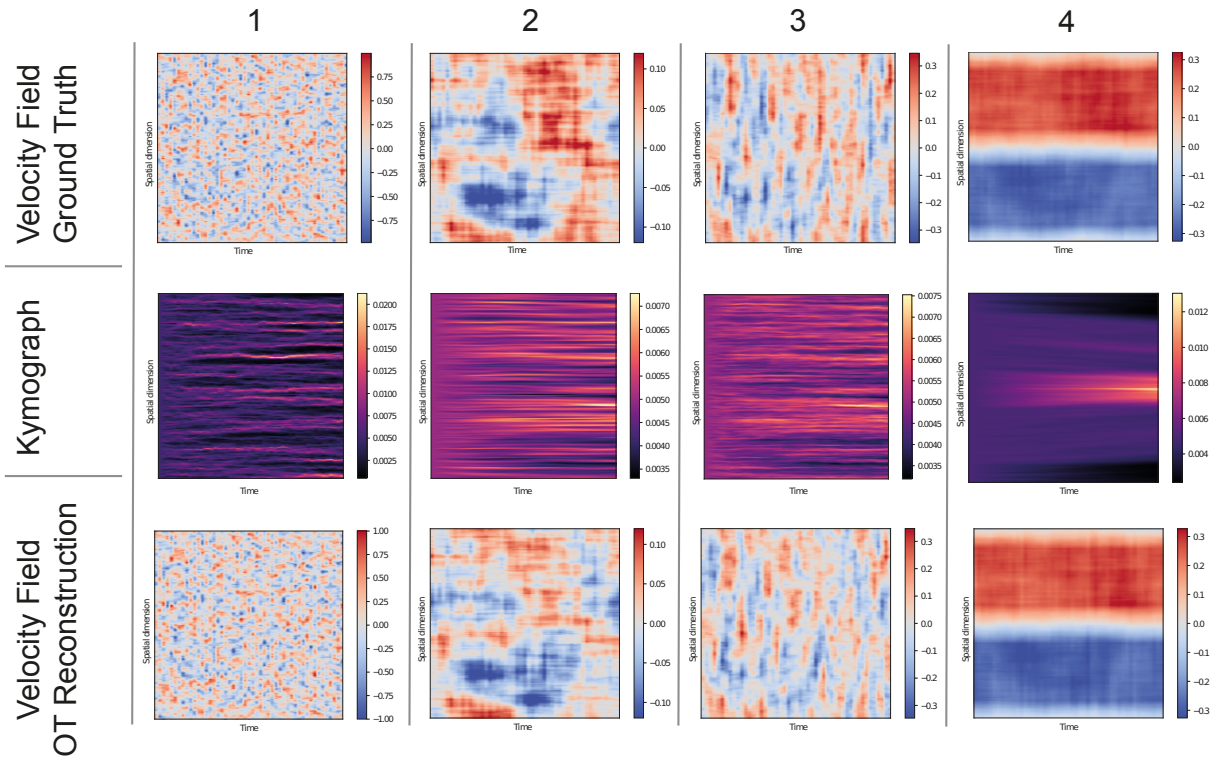

Numerical validation of the flow inference method on various simulated velocity fields.

1.4 Applications to neutrophil-like HL60 cells

1.4.1 Lipid membrane flows

For each cell, we generated an individual kymograph, from which we performed the flow inference using optimal transport (see image bellow). Velocity fields were then averaged across all our movies (Fig. 4B).

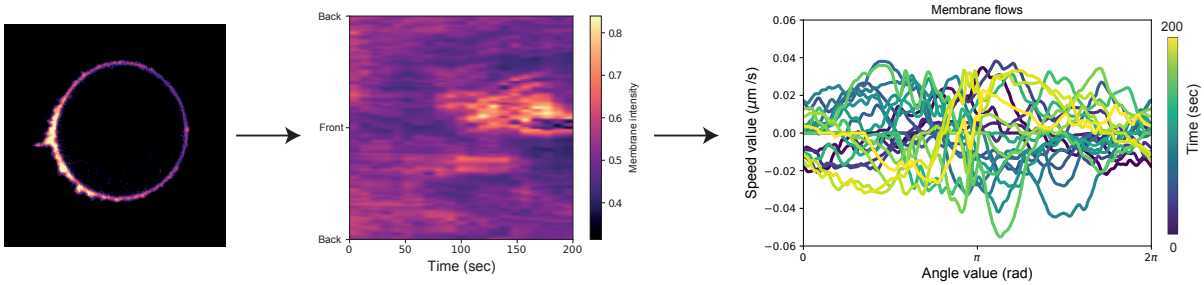

Kymographs are generated from timelapse microscopy images, and are used to infer velocity fields

We proposed an alternative representation of the flow (Fig. 4E) by representing it with arrows of length that scales with the intensity of the displacement measured (i.e with the speed of the flow): anterograde flows (from back to front) were displayed in red while retrograde flows were displayed in blue. We see clearly three phases: t=20 sec: Before illumination, nothing happens, there is a residual noise that is averaged across all the samples, which make the velocity really small. t=70sec During and Right After illumination: there is a anterograde flows, very fast and very intense. t=170sec. A retrograde flow, more progressive, restores the initial configuration of a uniformly distribution of membrane.

We provide a (Jupyter Notebook) and the original data for reproducibility on Github.

1.4.2 Cortical actin flows

We reproduce this procedure with actin. We generated kymographs of actin for each cells, and velocity fields from these kymographs. Velocity fields are then averaged across cells (Fig. S4G). We see the same behavior than with membrane flows: anterograde and then retrograde flows (Fig. S4K). We provide a (Jupyter Notebook) and the original data for reproducibility on Github.

2 Composite membrane-cortex mechanical model

2.1 Model hypotheses

We model the cell surface as a composite structure composed of a viscous active actomyosin cortex linked to an elastic membrane by adhesion proteins anchored in the cortex, as represented on the sketch below. The force transmission between membrane and cortex is mediated by a friction term. Our model hypotheses are directly inspired by the picket fence theory of the plasma membrane [6].

To simplify the description of the cortex-membrane interaction and exploiting the axisymmetry of the problem, we derive a minimal one-dimensional model of the composite cortex-membrane cell surface. We don't expect any of our results to be qualitatively different than with a more realistic 2D model of the membrane.

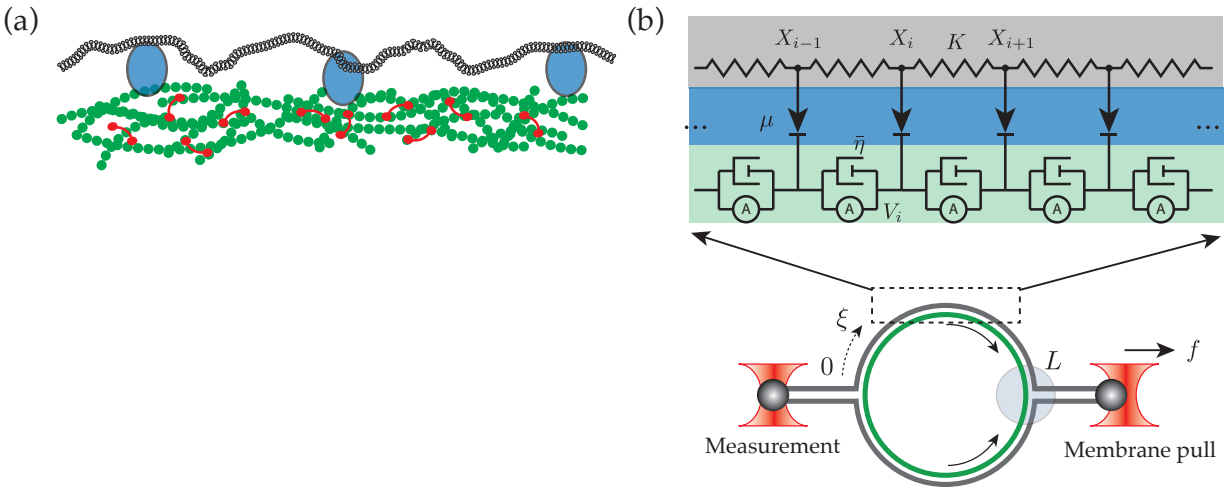

Sketch of the composite membrane-cortex structure and its mechanical representation. (a) Membrane-cortex structure. The plasma membrane is a passive bilayer that is attached to the cortex via adhesive molecules (blue ellipses) that are firmly attached to the cortex but can tangentially flow along the bilayer. (b) Schematic representation of the cortex-membrane structure. Assuming a axisymmetric geometry of the system, we can use a one-dimensional model for the cell surface. Multiple optical traps are used for both application and measurement of force. Cortical flows (arrows) may arise from localized light-based protein activation.

From a physical perspective, the mechanical response of the membrane is supposed linearly elastic at the macroscopic level. Our membrane therefore effectively resists stretching (and compressive) stress. This effective mechanical model of the membrane mechanics is justified by the entropic nature of the membrane tension [7]. The membrane should indeed be seen, at the microscopic level, as a highly folded structure (Fig. 6A in the main text and sketch below), where the folding is controlled by the competition between (Brownian and active) membrane fluctuations and bending rigidity. This competition leads to a macroscopic tension, which was shown to be exponential in the areal strain, both experimentally [8] and theoretically (starting from a classical Helfrich model) [9]. Here, we hypothesise small strains and we work therefore in the linear regime of the exponential, where we can approximate the membrane (in 1D) as a series of linear springs. Although the endogenous or exogenous perturbations we apply to the membrane do not lead to compressive stresses, one may note that a negative tension is also possible [7] and was recently predicted

from experimental fluctuation measurements in a detailed composite model of the red blood cell membrane and spectrin cytoskeleton [10].

The cortex is a contractile viscoelastic material, with a Maxwellian-like behavior, where the cortex flows as a viscous fluid on timescales larger a typical viscoelastic time $\tau \sim 10$s [11]. Our experiments are performed on timescales $t \sim 100$s, so we treat here the mechanical response of the cortex as essentially viscous. We model therefore the cortex as a thin layer of viscous active-gel [12], where we neglect polar or nematic order as in [13]. Here, we suppose the thickness T_0 of the cortex constant and define a 2-dimensional viscosity $\eta = T_0\eta_{3D}$.

Our cortex-membrane structure is modeled as an unfolded straight line of spatial coordinate $\xi \in [0, L]$, where L is the curvilinear length of the structure. We first write our model in a discrete setting[1], where we subdivide the structure into N elements of size L/N, labelled by an index i. Then we coarse-grain the equations into an equivalent continuous formulation that is better adapted to be solved through finite-element simulations.

The discrete model of the membrane consists of a chain of elastic springs with elastic constant $K[N/m]$. To each spring i it is associated a displacement field X_i. The actomyosin cortex is also represented here in its discrete form using a phenomenological model for the contractility, in which the rheology of the cortex is equivalent to the parallel association of a contractile element and a dashpot, representing the viscous dissipation [14]. Such an element is characterized by an active tension σ_i, a bulk viscosity η_{3D} and a velocity field V_i. The membrane-cortex interaction is ensured by the presence of cortex-bound proteins that are linked to the plasma membrane but allow for relative motion to the cortex, which generates frictional forces proportional to the relative velocity between the membrane and cortex and characterized by a friction coefficient $\bar{\mu}$.

2.2 Mechanical equations of the composite membrane

The system of equations that govern the dynamics of this system derives from force balance in both the cortex and the membrane.

2.2.1 Discrete equilibrium equations

To obtain the mechanical equilibrium at a position X_i in the membrane we consider the force balance between the elastic response of the membrane and the friction force arising from cortex-membrane interaction. The discrete equation at a node i reads

$$K(X_{i+1} - 2X_i + X_{i-1}) + \bar{\mu}(V_i - \dot{X}_i) = 0, \tag{6}$$

where $\bar{\mu}[N.s/m]$ is the friction coefficient of the cortex-membrane interaction, V_i is the velocity field of the cortex at node i, and $\dot{X}_i$ is the time-derivative of the membrane's displacement field.

Analogously, we can write down the equilibrium for an element i in the cortex. Let $\eta_{3D}[Pa.s]$ be the three-dimensional effective viscosity of the actomyosin gel of constant thickness T_0, and let define a characteristic cross area element $\delta A = T_0 h$, where h is a characteristic transversal length. The force due to the viscous deformation of the cortex is $\delta A \eta_{3D} \partial V_i/\partial\xi$. The balance of forces at the element i reads then

$$\delta A\, \eta_{3D}\left(\frac{\partial V_{i+1}}{\partial \xi} - \frac{\partial V_i}{\partial \xi}\right) + \delta A(\sigma_{i+1} - \sigma_i) + \bar{\mu}(\dot{X}_i - V_i) = 0 \tag{7}$$

2.2.2 Continuum limit

In the continuum limit, we substitute the discrete derivatives $X_{i+1} - X_i = h\partial x(\xi)/\partial\xi$, where $h = L/N$ is the discrete spacing and tends to zero as $N \to \infty$. Let $\mu = \bar{\mu}/h^2[N.s/m^3]$ represent the local friction density. For notation uniformity, the elastic constant K is written as $k \equiv K[N/m]$. We can write a continuum analog

[1] Note that both cortex and membrane share the same spatial coordinates. In a discrete setting, this means that a particular spatial point will correspond to the same index i for both cortex and membrane.

of (6) as,

$$\begin{aligned} k\frac{\partial^2 x}{\partial \xi^2} - \mu(\dot{x} - v) = 0, \\ x(\xi = 0) = 0,\ x(\xi = L) = \tilde{x}. \end{aligned} \tag{8}$$

Notice that we enforce a Dirichlet boundary condition on the displacement at $\xi = 0$ such that the displacement field is zero to ensure the symmetry of the model. We further suppose that the mechanical perturbation applied by the optical trap can be modelled by an additional Dirichlet boundary condition at $\xi = L$.

The continuum analog of (7) is

$$\eta\frac{\partial^2 v}{\partial \xi^2} + \frac{\partial \sigma_{active}}{\partial \xi} - \mu(v - \dot{x}) = 0, \tag{9}$$

where $\eta = T_0\eta_{3D}[Pa.s.m]$ is the two-dimensional effective viscosity of the cortex[2].

The system can be seen as a one-dimensional representation of a axisymmetric system. It is easy to visualise that if a localized contraction happens somewhere in the cell, there will be always a point in the cell in which the cortical flows are identically zero because of symmetry. Our one-dimensional representation is then seen as the "unwrapping" of such system into a one-dimensional string, where we enforce the boundary conditions $v(\xi = 0) = 0$, and $v(\xi = L) = \bar{v}$, where $\bar{v}$ is the velocity of protuding membrane at the cell front in response to light activation.

2.2.3 Final system of mechanical equations

The cortex-membrane system is represented by a coarse-grained model in which the membrane state is fully characterized by the scalar *displacement* field x, while the cortex is described by the scalar *velocity* field v. The one-dimensional spatial domain is $\Omega \in [0, L]$, and we observe the sytem at a time $t \in (0, T]$. Dividing both equations (8) and (9) by μ, the final system of equations describing the system dynamics reads

$$\frac{\partial x}{\partial t} + \frac{\eta}{\mu}\frac{\partial^2 v}{\partial \xi^2} + \frac{1}{\mu}\frac{\partial \sigma_{active}}{\partial \xi} - v = 0, \qquad \text{in } \Omega \times (0, T] \tag{10a}$$

$$\frac{\partial x}{\partial t} - \frac{k}{\mu}\frac{\partial^2 x}{\partial \xi^2} - v = 0, \qquad \text{in } \Omega \times (0, T] \tag{10b}$$

$$x(\xi = 0) = 0, \text{ and } x(\xi = L) = \tilde{x} \qquad \text{on } \partial\Omega \times (0, T] \tag{10c}$$

$$v(\xi = 0) = 0, \text{ and } v(\xi = L) = \tilde{v} \qquad \text{on } \partial\Omega \times (0, T] \tag{10d}$$

One may identify three main parameters controlling the system dynamics:

- A hydrodynamic length $\lambda = \sqrt{\eta/\mu}$, which compares membrane friction and cortex viscous forces and corresponds to the typical length above which cortical flows may be dampened by membrane-cortex friction, and to be compared with the system lenght L.
- A characteristic timescale $\tau = \eta/k$, which compares the elastic membrane force with the cortical viscous force.
- A dimensionless cortex pulling velocity $\bar{\tilde{v}} = \tilde{v}\frac{\tau}{\lambda} = \tilde{v}\frac{\sqrt{\eta\mu}}{k}$.

Note that, only spatial gradients, but not the absolute value of the cortical tension $\gamma = T_0\sigma_{active}$ does play a role in the system response dynamics.

[2]Notice that we use lowercase letters x, v when describing continuum variables, while uppercase X_i, V_i will be reserved for discrete variables

These length and time-scales could allow us to non-dimensionalize the system above in the following form

$$\begin{aligned}
&\frac{\partial \bar{x}}{\partial \bar{t}} + \frac{\partial^2 \bar{v}}{\partial \bar{\xi}^2} + \frac{\partial \bar{\sigma}_{active}}{\partial \bar{\xi}} - \bar{v} = 0, && \text{in } \Omega \times (0, \bar{T}] \\
&\frac{\partial \bar{x}}{\partial \bar{t}} - \frac{\partial^2 \bar{x}}{\partial \bar{\xi}^2} - \bar{v} = 0, && \text{in } \Omega \times (0, \bar{T}] \\
&\bar{x}(\bar{\xi} = 0) = 0, \text{ and } \bar{x}(\bar{\xi} = \bar{L}) = \bar{\tilde{x}} && \text{on } \partial\Omega \times (0, \bar{T}] \\
&\bar{v}(\bar{\xi} = 0) = 0, \text{ and } \bar{v}(\bar{\xi} = \bar{L}) = \bar{\tilde{v}} && \text{on } \partial\Omega \times (0, \bar{T}],
\end{aligned}$$

We decided to keep dimensionalized equations for easier physical interpretation.

2.3 Numerical implementation

Because we have a time-dependent system of partial differential equations (PDEs), we first discretize in time by a finite difference approximation, which yields a sequence of stationary problems, and then turn each stationary problem into a variational formulation. From now on, the derivative with respect to the spatial coordinate ξ will be denoted by $\nabla \equiv \partial/\partial\xi$.

2.3.1 Time discretization

In order to solve (11), for the displacement $x(\xi, t)$ and velocity $v(\xi, t)$, we first discuss the time discretization. We use the superscript n to denote a quantity at discrete timesteps $t^n = n\Delta t$, where $n = 0, 1, 2, \ldots$. For an arbitrary field $\phi(\xi, t)$, $\phi^n = \phi(\xi, t = t^n)$. A finite difference implicit discretization in time first consists of sampling the PDE system at some time, say t^{n+1}:

$$\left(\frac{\partial x}{\partial t}\right)^{n+1} + \frac{\eta}{\mu}\nabla^2 v^{n+1} + \frac{1}{\mu}\nabla\sigma_{active}^{n+1} - v^{n+1} = 0, \tag{12a}$$

$$\left(\frac{\partial x}{\partial t}\right)^{n+1} = \frac{k}{\mu}\nabla^2 x^{n+1} + v^{n+1}. \tag{12b}$$

The time-derivative is then approximated by a difference quotient. For simplicity and stability reasons, we chose a simple backward Euler method:

$$\left(\frac{\partial x}{\partial t}\right)^{n+1} \approx \frac{x^{n+1} - x^n}{\Delta t}, \tag{13}$$

where Δt is the time discretization parameter.

2.3.2 Variational formulation

Let $\hat{x}$, and $\hat{v}$ be the test functions. We first approximate the time derivatives using (13), then mutiply each equation by tests function, integrate over the spatial domain Ω, and sum the equations.

$$\begin{aligned}
\int_\Omega (\Delta t^{-1}(x^{n+1} - x^n)\hat{v} + \frac{\eta}{\mu}\nabla^2 v^{n+1}\hat{v} + \frac{1}{\mu}\nabla\sigma_{active}^{n+1}\hat{v} - v^{n+1}\hat{v})d\xi \\
+ \int_\Omega (\Delta t^{-1}(x^{n+1} - x^n)\hat{x} - \frac{k}{\mu}\nabla^2 x^{n+1}\hat{x} - v^{n+1}\hat{x})d\xi = 0
\end{aligned} \tag{14}$$

Integration by parts allows us to write,

$$\begin{aligned}
\int_\Omega (\Delta t^{-1}(x^{n+1} - x^n)\hat{v} - \frac{\eta}{\mu}\nabla v^{n+1}\nabla\hat{v} + \frac{1}{\mu}\nabla\sigma_{active}^{n+1}\hat{v} - v^{n+1}\hat{v})d\xi \\
+ \int_\Omega (\Delta t^{-1}(x^{n+1} - x^n)\hat{x} + \frac{k}{\mu}\nabla x^{n+1}\nabla\hat{x} - v^{n+1}\hat{x})d\xi = 0.
\end{aligned} \tag{15}$$

2.3.3 Finite-element implementation

At each time step, we solve (15) for the cortex velocity field v, and membrane displacement x. We assume a quadratic continuous (P2-Lagrange finite-element) interpolation for the velocity field v, and x. The dynamic evolution is solved using a backward Euler method.

Aiming at facilitating the spread, modification, refinement of our model and to highlight its features, we furthermore devise a numerical scheme (available on GitHub) to solve the system of partial differential equations with the finite-element library FEniCS [15].

2.3.4 Control case: constant contractility

As a validation for our finite element implementation of the coupled system of equations and boundary conditions, we compare the results of our code against a simplified setting where analytical solutions are possible. The simplest case assumes a uniform contractile stress, and we set $v = 0$ to solve the membrane equilibrium equation

$$\begin{aligned} &\frac{\partial x}{\partial t} = \frac{k}{\mu}\frac{\partial^2 x}{\partial \xi^2}, \qquad (\xi, t) \in [0, L] \times (0, \infty) \\ &x(\xi, t = 0) = 0 \\ &x(\xi = 0, t) = h(t). \end{aligned} \tag{16}$$

which is similar to a heat equation with boundary conditions. Such equation has a closed analytical solution

$$x(\xi, t) = \int_0^t \frac{\xi}{\sqrt{4\pi\lambda(t-s)^3}} e^{-\frac{\xi^2}{4\lambda(t-s)}} h(s) dy, \tag{17}$$

where $k/\mu = \lambda$.

Numerically, we need to decouple the membrane equilibrium equations from the cortex. This is achieved by setting $\mu \to 0$. Because (16) only depends on the ratio k/μ, we make the limit $\mu \to 0$, and $k \to 0$, such that $k/\mu \to 1$. The comparison between analytical results and finite element simulations shows good agreement, as shown below

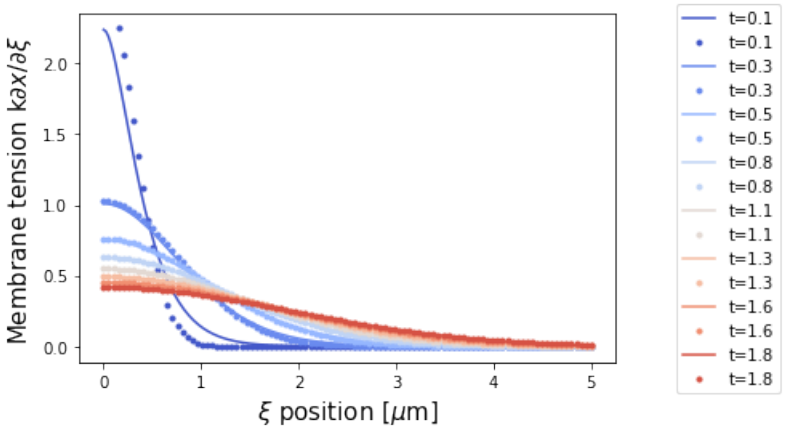

Membrane tension profiles along the membrane for increasing times. Continuous line: analytical solution based on (17). Points: finite element solution of (15).

2.4 Numerical values

The physical values used in the simulations are summarized in the table below. The membrane elasticity [N/m] is estimated based on the membrane tension, which can be obtained by pulling membrane tethers from the plasma membrane using laser tweezers [16]. The friction coefficient here is estimated as $\mu = \zeta\rho_0$, where $\zeta \approx 10^-6$ Pa.s.m [17] is the drag resistance of an individual linker and $\rho = 10^{14} m^{-2}$ is the surface density of linkers [18].

Notation	Quantity	Experimental Value	Ref(s).
$R = L/\pi$	Neutrophil cell radius	5-6μm	
k	membrane elasticity	10 - 100 pN/μm	[16]
η_{3D}	Actomyosin shear viscosity	$10^4 - 10^5$Pa s	[13]
μ	Friction coefficient	100 pN.s/μm^3	[17,18]
T_0	Cortex thickness	200nm	[19]
$\eta = \eta_{3D} T_0$	2D effective viscosity	2×10^4 pN.s/μm	
$\lambda = \sqrt{\frac{\eta}{\mu}}$	Hydrodynamic length	30 - 100 μm	
$\tau = \eta/k$	Characteristic timescale	200 - 2000 s	

Table of numerical values.

2.5 Results

We provide a (Jupyter Notebook) with the code and implementation for figures in the main text (Fig. 6B,C) and figures for the control above and for the role of friction (see below).

In the article, we are mainly interested in understanding how the membrane (i.e. lipid bilayer) tension propagates along the cell. There are two main cases of interest. In the "exogenous perturbation", the plasma membrane is pulled by an optical trap at the cell front and a membrane force is measured by an optical tweezer at the other end (back of the cell). In the so-called "endogenous perturbation", we used an optogenetic tool to locally generate and actin-driven cellular protrusion of velocity $\tilde{v}$ at the cell front and we measure the instantaneous resulting membrane tension at the back. The local membrane tension measured by an optical trap may be defined as $k\frac{\partial x}{\partial \xi}$.

Exogenous perturbation

We modelled the perturbation on the membrane by an optical trap as a Dirichlet boundary condition on the displacement field $x(\xi = L, t)$. The perturbation propagates along the cell because of the elasticity of the membrane, however, the viscous dissipation of the membrane-cortex interaction buffers such propagation. It is important to notice that the observational timescale (The time at which the membrane tension is observed) is crucial. Since the membrane is considered to be linearly elastic, in the limit $t \to \infty$, the tension becomes uniform across the whole cell. Here we chose to solve the system up to some observational time t_f. In the figure below, we illustrate a scheme for the exogenous perturbation, where a cell is pulled at one end and we observe the force propagation along the system.

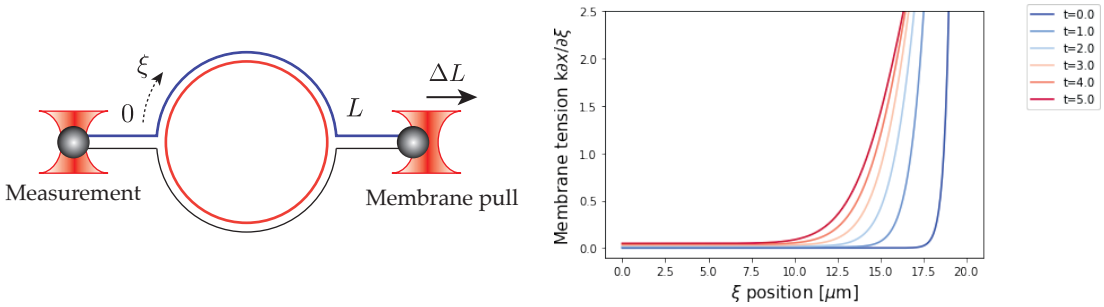

Exogenous perturbation. Sketch of the system (left) and membrane tension profiles [nN] for increasing times after the perturbation (right). Refer to GitHub for the set of physical parameters and procedure.

Endogenous perturbation

The endogenous force generation can be modelled in two different ways providing same qualitative features. First, as an active source of contraction via the term σ, or via a Dirichlet boundary condition on the velocity field $v(\xi = L, t) = \bar{v}$, which is used here for simplicity. The boundary condition is complemented with a full clamp at $\xi = 0$, and by unconstraining the membrane at $\xi = L$. As in the endogenous case, here we need

to specify an observational time, which is linked to the fact that the contractility is happening at a definite, finite, time interval.

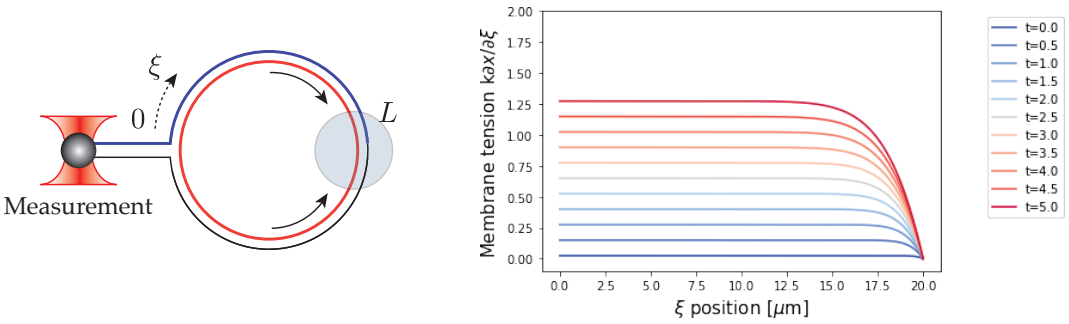

Endogenous perturbation. Sketch of the system (left) and membrane tension profiles [nN] for increasing times after the perturbation (right). Refer to GitHub for the set of physical parameters and procedure.

The role of friction

A key factor in the system is the role of the cortex-membrane friction, that is proportional to the relative particle velocity between the cortex and membrane and is expected to be proportional to the surface density of membrane-cortex linkers.

In the case of an **exogenous perturbation**, a perturbation in the membrane will propagate as in a elastic solid in the limit of low friction, $\mu \to 0$, and the membrane tension will be uniform across the cell. In the high friction limit $\mu \gg 1$, the perturbation is dissipated along the cell and the force is not propagated at finite observational time, as shown on panel (a) of the figure below. Furthermore, the cortex viscosity plays here an important role in dampening the tension propagation, as illustrated in the panel (b) of the figure below.

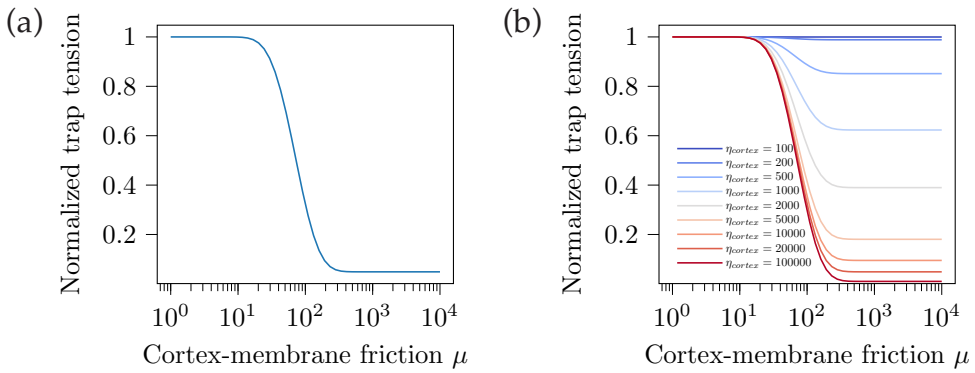

Normalized membrane tension for an exogenous perturbation as a function of the cortex-membrane friction (a) Normalized membrane tension profile for a cortex viscosity $\eta = 100000$ pN.s/mum . (b) Normalized membrane tension profiles for increasing cortical viscosities $\eta = 10^2 - 10^5$. Refer to GitHub for the whole set of physical parameters and procedure. The tension is normalized by its max value (tension = tension/max tension).

In the case of an **endogenous perturbation**, force transmission behaves depends on the cortex-membrane friction in a different manner. In the low friction $\mu \to 0$, the cortex does not interact with the membrane, meaning that cortical flows will not generate membrane stresses. In the high friction limit $\mu \gg 1$, cortical flows will drag the membrane transmitting the tension, as shown on the figure below.

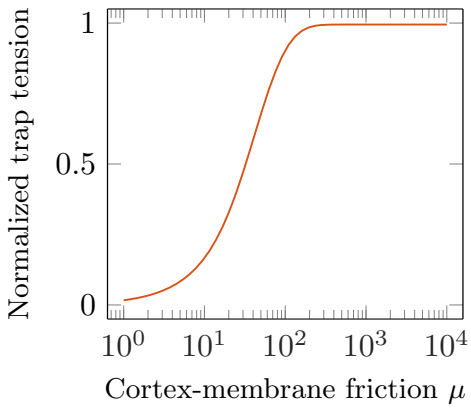

Normalized membrane tension for an endogenous perturbation as a function of the cortex-membrane friction. Refer to GitHub for the set of physical parameters and procedure. The tension is normalized by its max value.